

Supplementary Materials

Hydrogen-bond guided micellar self-assembly directed carbon superstructures towards high-energy and ultralong-life zinc-ion hybrid capacitors

Shreeti Jha,^a Yang Qin,^a Yumin Chen,^a Ziyang Song,^a Ling Miao,^{*a} Yaokang Lv,^c Lihua Gan,^{*a, b} and Mingxian Liu^{*a, b}

^a*Shanghai Key Lab of Chemical Assessment and Sustainability, School of Chemical Science and Engineering, Tongji University, 1239 Siping Rd., Shanghai, 200092, P. R. China.*

^b*State Key Laboratory of Cardiovascular Diseases and Medical Innovation Center, Shanghai East Hospital, School of Medicine, Tongji University, 150 Jimo Rd., Shanghai 200120, P. R. China.*

^c*College of Chemical Engineering, Zhejiang University of Technology, Hangzhou 310014, P. R. China.*

*Corresponding Authors

E-mail: 22169@tongji.edu.cn (L. Miao), ganlh@tongji.edu.cn (L. Gan), liumx@tongji.edu.cn (M. Liu).

1. Experimental Section

1.1 Chemicals and Materials

Tetrachloro-1, 4-benzoquinone ($C_6Cl_4O_2$), 4, 4'-methylenedianiline ($CH_2(C_6H_4NH_2)_2$) and 1, 4-dioxane were purchased from Adamas-Beta, ethanol (C_2H_6O), sodium amide ($NaNH_2$) was purchased from general reagent, triblock poly (ethylene oxide)-b-poly (propylene oxide)-b-poly (ethylene oxide) Pluronic F127 ($M_{av} = 12600$) were purchased from Sigma-Aldrich. All chemicals were analytical grade and utilized without further purification. Deionized water was utilized in all experiments.

1.2 Synthesis

First of all, 4, 4'-methylenedianiline (MDA) (10 mmol) with 2 g F127 was dissolved in 50 ml 1, 4-dioxane to form MDA solution, and 5 mmol of tetrachloro-1, 4 benzoquinone (TB) was also dissolved in another 50 ml 1, 4 dioxane. Secondly, MDA solution was added dropwise into TB solution contained in round bottom flask at room temperature with vigorous stirring about 20 min. Thirdly the mixture was transferred into a Teflon-inner autoclave for hydrothermal polymerization at 100 °C for 12 hours. After filtration, washing with 1, 4-dioxane and ethanol respectively, the polymer (i.e. poly(TM)) was obtained. The obtained poly(TM) and $NaNH_2$ as activator with mass ratio of 1:1 was mixed and pyrolyzed at 750°C for 2 h in N_2 atmosphere with heating rate of 3°C min⁻¹. The obtained products after carbonization and activation were washed several times with deionized water to remove the impurities. Poly(TM) derived carbon

superstructures (CS- x , x represents the carbonization and activation temperature) were also prepared with the same procedure at different pyrolysis temperature.

1.3 Characterization

The morphology and structure of carbon materials were observed using scanning electron microscope (SEM, JSM-7900F) and transmission electron microscopy (TEM, JEM-2100). The surface element composition and state of the products were studied using X-ray photoelectron spectrometer. Nitrogen sorption and desorption isotherms were measured using Micromeritics of ASAP 2460 apparatus at $-196\text{ }^{\circ}\text{C}$. The specific surface area and pore size distribution were calculated using Brumanuer-Emmett-Teller method and Nonlocal density functional theory, respectively. X-ray diffraction technique (XRD) was used to characterize the phase structure of materials. Raman spectroscopy (Renishaw Invia, the laser excitation $\lambda = 514\text{ nm}$) was used to analyze graphitization degree of carbon materials.

1.4 Electrochemical evaluation

The working electrodes were prepared by mixing a mixture slurry consisting of CS- x materials, graphite, polytetrafluoroethylene (PTEE) binder at a mass ratio of 8: 1: 1 soaked in ethanol. The mixture was dispersed by ultrasound for 2 h then dried in oven at $100\text{ }^{\circ}\text{C}$ for 12 h. Dried mixture was pressed on stainless steel mesh, with mass loading of active carbon material of 3 mg cm^{-2} . The aqueous zinc-ion hybrid capacitor (ZHCs) was assembled with Zn foil as anode, working electrode as cathode, $3\text{M Zn (CFSO}_3)_2$ as the electrolyte and glassy fibrous as separator.

Galvanostatic charging/discharging (GCD) tests were performed on CT3001A battery test system with potential range of 0 to 1.8 V. The cyclic voltammetry (CV) and electrochemical impedance spectroscopy (EIS) were studied through CHI660E electrochemical workstation. The specific capacity (C_m , mAh g⁻¹) of the working electrode was calculated by the equation (1):

$$C_m = \frac{I \times \Delta t}{m} \quad (\text{Eq. S1})$$

Where I refer to the current density (A g⁻¹), Δt represents the discharging time (s) and m (g) is the mass loading of the active substance. Energy Density (E , Wh kg⁻¹) and power density (P , W kg⁻¹) were calculated based on the following equations:

$$E = C_m \times \Delta V \quad (\text{Eq. S2})$$

$$P = \frac{C_m \times \Delta V}{1000 \times \Delta t} \quad (\text{Eq. S3})$$

S3)

Where ΔV is the voltage window.

1.4 Ion diffusion Behavior

The relaxation time constant (τ_0) was calculated from reciprocal of the frequency (f , Hz):

$$\tau_0 = 1/f \quad (\text{Eq. S4})$$

The combined series resistances (R_s) were calculated from the intersection of the curve and horizontal axis, having electrode/electrolyte interface resistance, electrolyte ionic resistance and active material electronic resistance. The charge transfer resistance (R_{ct}) is the radius of semicircle in the curves of Nyquist plot.

The ion diffusion coefficient (D , $\text{cm}^2 \text{s}^{-1}$) was calculated by the equation:

$$D = \frac{R^2 T^2}{2A^2 C^2 F^4 n^4 \sigma^2} \quad (\text{Eq. S5})$$

Where R ($8.314 \text{ J mol}^{-1} \text{ K}^{-1}$) is gas constant, T (293.15 K) is Kelvin temperature, A ($\text{m}^2 \text{ g}^{-1}$) is the surface area of the electrodes, c (mol L^{-1}) is molar concentration of electrolyte, n is electron transfer numbers per molecule during electron reaction, F is the faraday constant and σ ($\Omega \text{ s}^{-0.5}$) is diffusive resistance.

1.5 Charge storage kinetics.

The ion and electron transport kinetics of the assembled ZHCs were investigated based on the equation:

$$i = kv^b \quad (\text{Eq. S6})$$

Where k and b are constants, i is current, and v resemble scan rate. The power exponent b is the key indicator for predicting charge storage kinetics. It is generally accepted that b -value of 0.5 denotes diffusion-controlled procedure whereas b -value of 1.0 denotes surface governed process.

The Dunn's method was used to analyze the capacitive contribution and the diffusion-controlled process, which were calculated by quantifying the relationship between i and v , using following equation:

$$i = k_1v + k_2v^{1/2} \quad (\text{Eq. S7})$$

Where k_1v represents the current density contributed from surface fast-capacitive process whereas $k_2v^{1/2}$ denotes for the diffusion-controlled process, both k_1 and k_2 are constants.

Dividing both sides by $v^{1/2}$ of the above equation gives following expression:

$$i/v^{1/2} = k_1v^{1/2} + k_2 \quad (\text{Eq. S8})$$

Generally, $i/v^{1/2}$ and $v^{1/2}$ shows linear relationship which was achieved by a linear fitting. The slope of straight line is equivalent to k_1 and the y-intercept corresponds to k_2 . The capacitive contributions were calculated quantitatively by repeating the preceding procedures for different voltage and scan rates.

2. Supplementary Characterizations

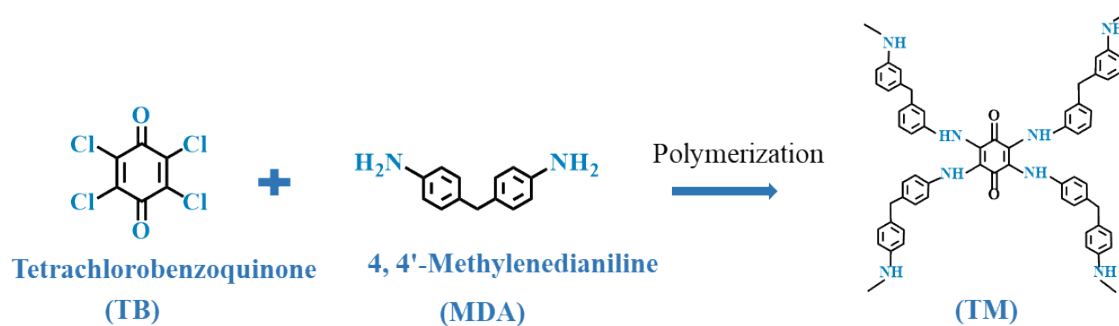


Figure S1. Synthesis route of carbon precursor via polymerization reaction.

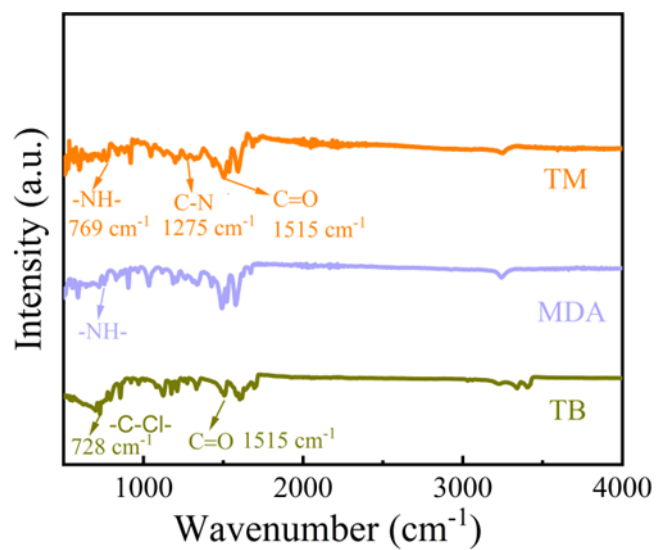


Figure S2. FT-IR spectra of TB, MDA and TM

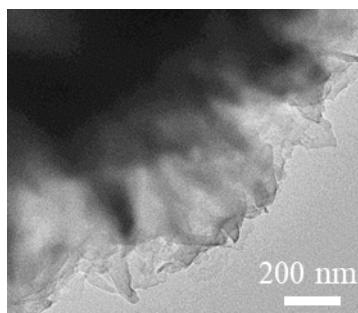


Figure S3. TEM image of CS-750 cathode.

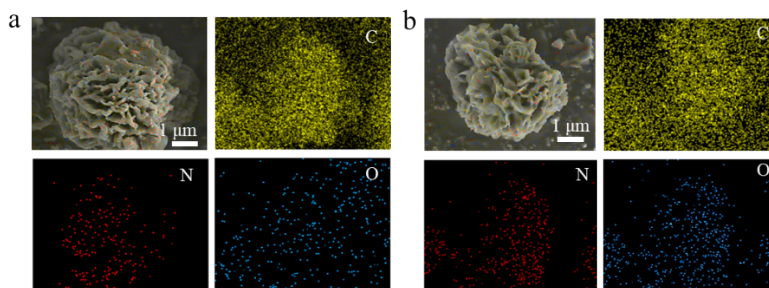


Figure S4. SEM image with element distribution on the surface: (a) CS-700 (b) CS-800

Table S1. Pore structure parameters of CS-*x* samples.

Sample	S_{BET} ($\text{m}^2 \text{g}^{-1}$)	S_{micro} ($\text{m}^2 \text{g}^{-1}$)	S_{meso} ($\text{m}^2 \text{g}^{-1}$)	V_{total} ($\text{cm}^3 \text{g}^{-1}$)	V_{micro} ($\text{cm}^3 \text{g}^{-1}$)	V_{macro} ($\text{cm}^3 \text{g}^{-1}$)	V_{meso} ($\text{cm}^3 \text{g}^{-1}$)	$V_{\text{meso}}/V_{\text{total}}$ (%)
CS-700	954	575	197	0.46	0.23	0.07	0.16	34.7
CS-750	2824	1369	1428	1.56	0.28	0.10	1.18	75.6
CS-800	1431	1001	430	0.81	0.34	0.06	0.41	50.6

S_{BET} , S_{micro} , S_{meso} , V_{total} , V_{micro} , V_{macro} , V_{meso} , $V_{\text{meso}}/V_{\text{total}}$ represents surface area, micro surface area, mesopore surface area, total pore volume, micropore volume, macropore volume and mesopore volume.

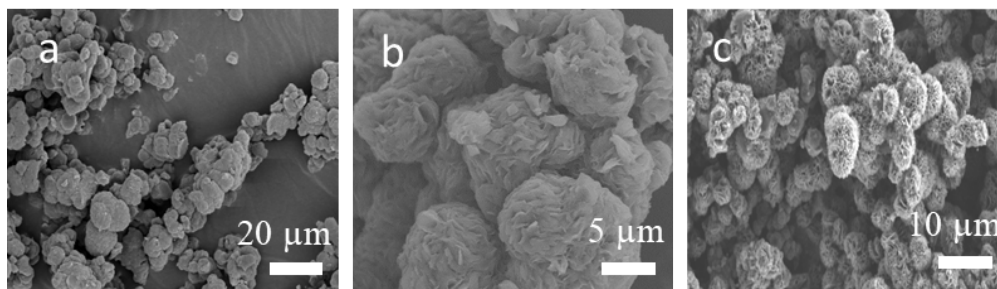


Figure S5. SEM images with different amount of F127: (a) 0 g, (b) 1 g, (c) 2 g.

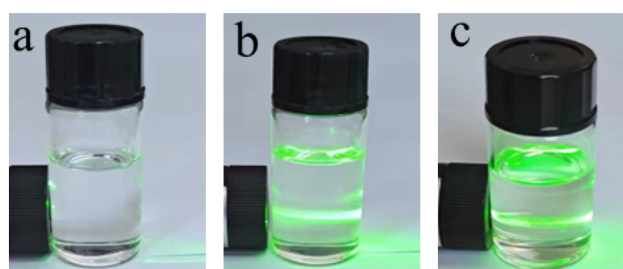


Figure S6. Pictures with different amount of F127 representing Tyndall effect: (a) 0 g F127, (b) 1 g F127 and (c) 2 g F127.

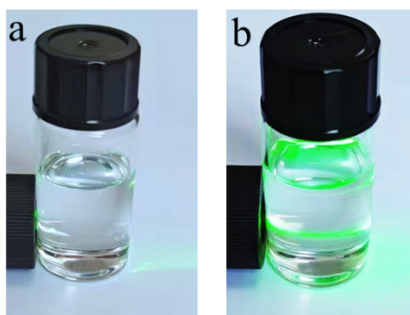


Figure S7. Pictures representing Tyndall effect at two different temperatures: (a) 25°C and (b) 100 °C

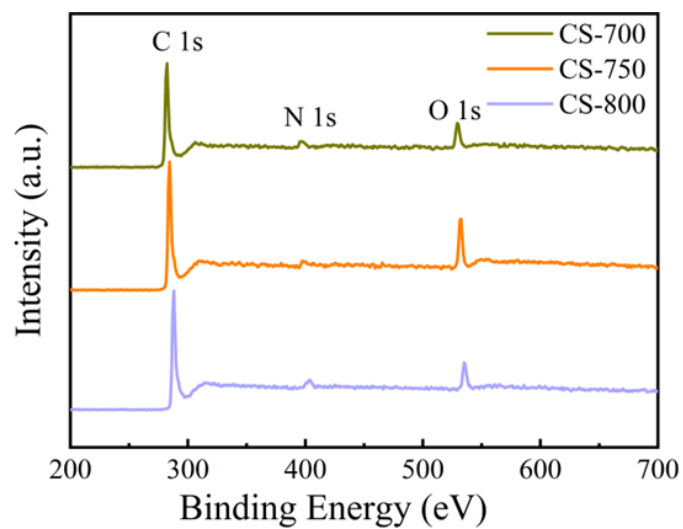


Figure S8. XPS spectra of CS-*x*

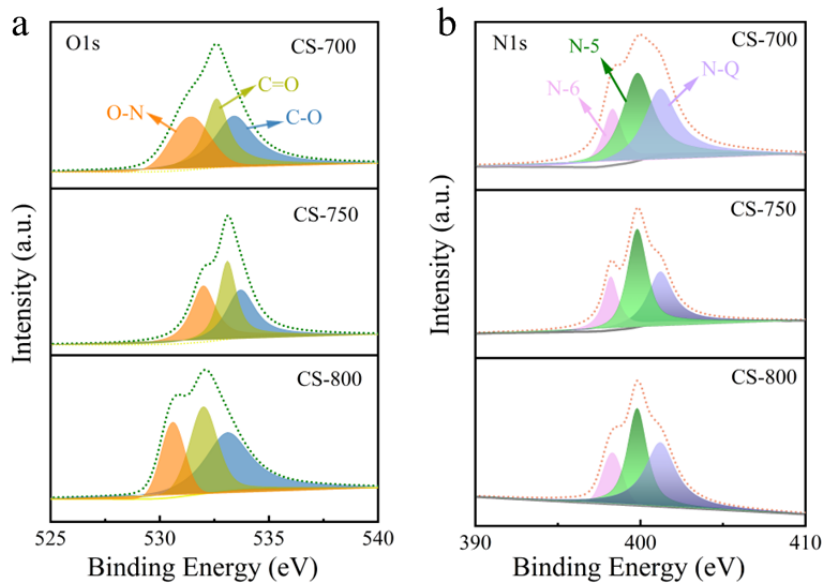


Figure S9. High resolution XPS spectra of CS-*x*: (a) O 1s, (b) N 1s.

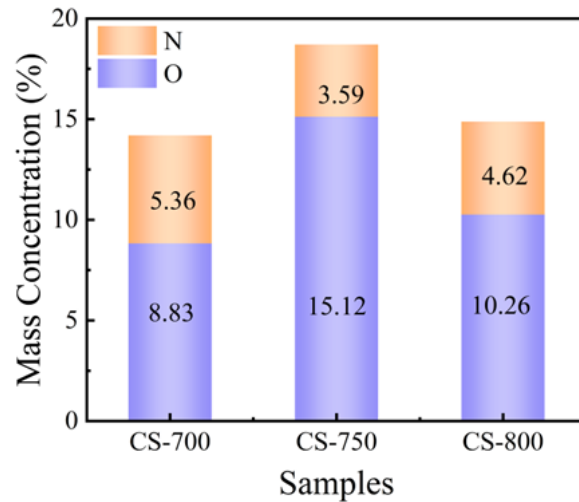


Figure S10. C, N, O content of CS-x obtained by XPS.

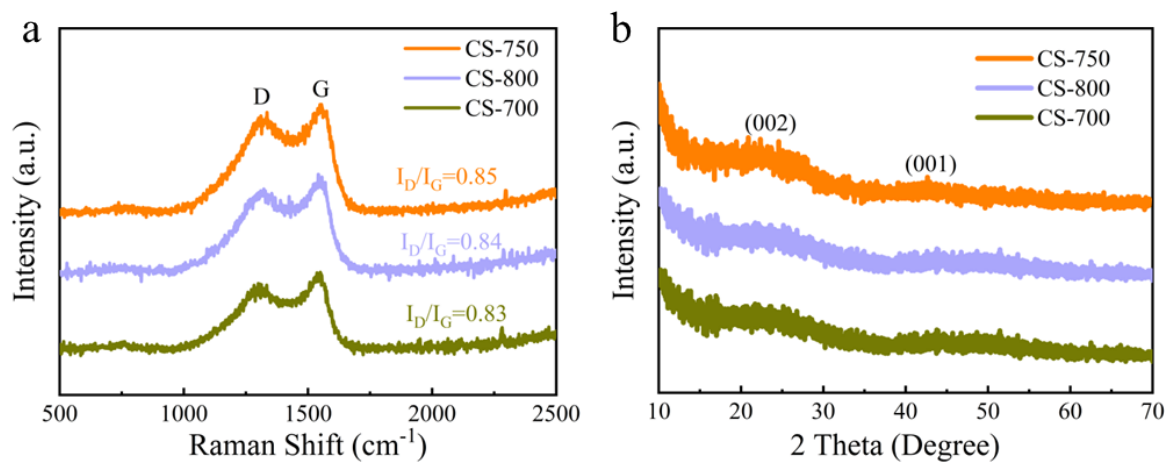


Figure S11. (a) Raman spectra (b) XRD patterns of CS-x.

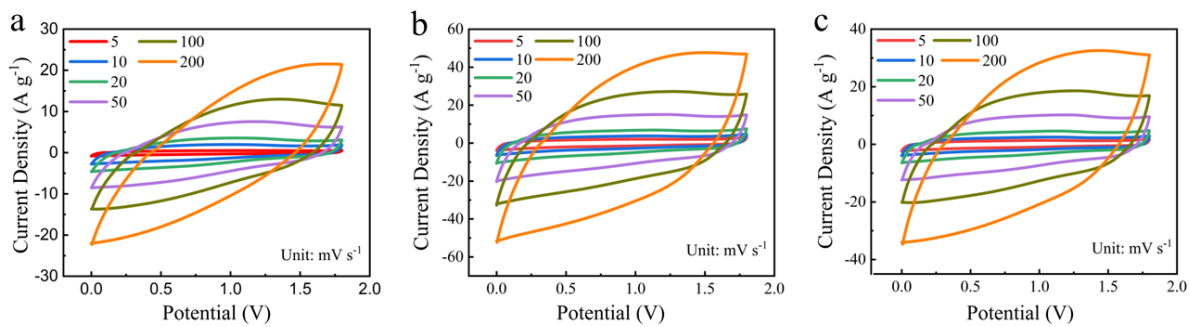


Figure S12. CV curves of CS-*x* device at different scan rates: (a) CS-700, (b) CS-750 and (c) CS-800.

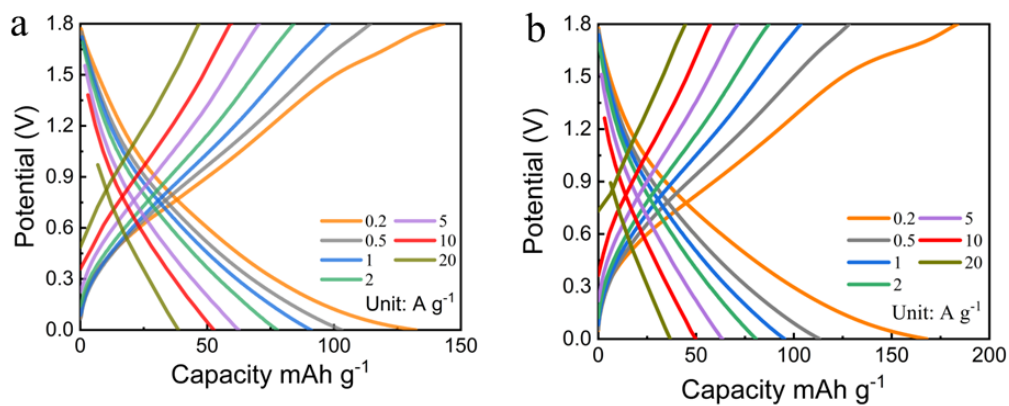


Figure S13. GCD curves of CS-*x* device: (a) CS-700 and (b) CS-800.

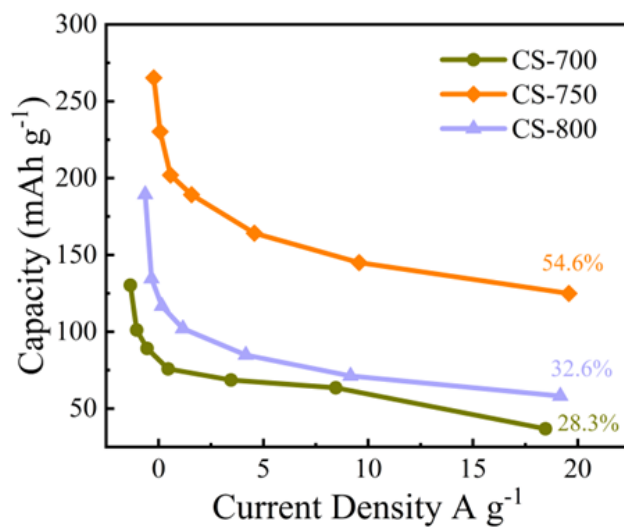


Figure S14. Rate capabilities of CS-x devices from 0.2 to 20 A g⁻¹.

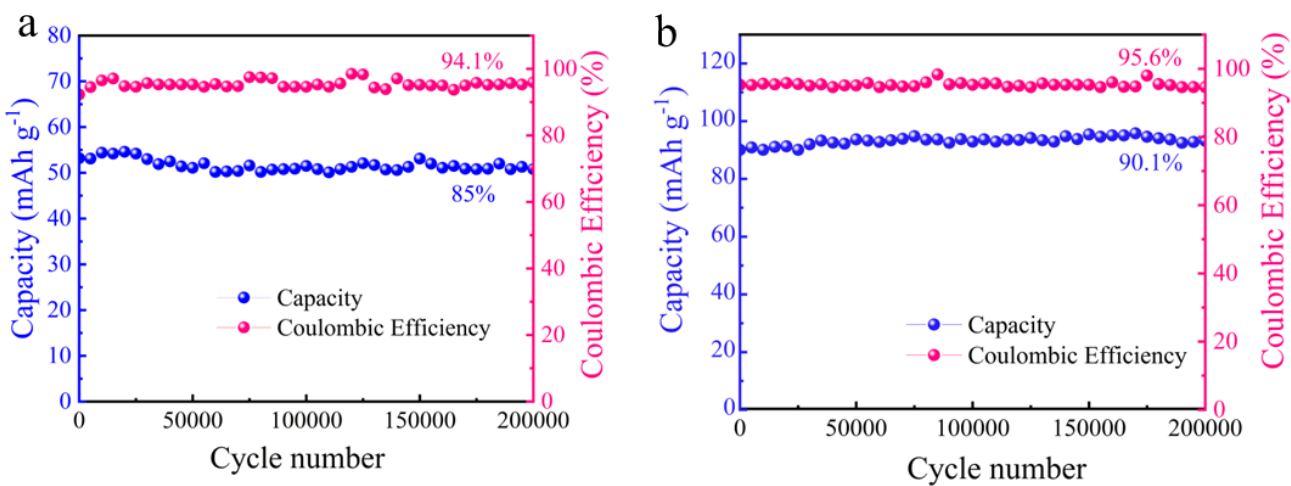


Figure S15. Cyclability and Coulombic efficiency of CS-x devices respectively: (a) CS-700, (b) CS-800.

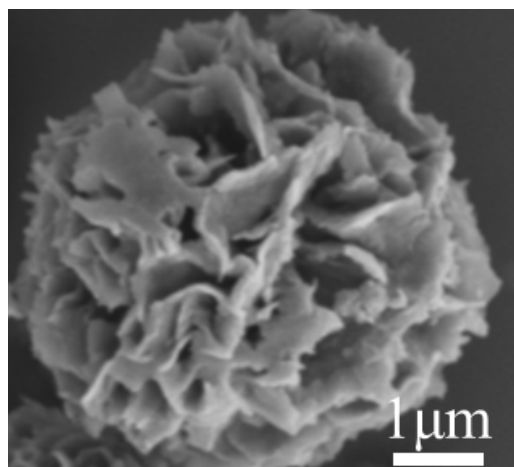


Figure S16. SEM image of CS-750 cathode after 200, 000 cycles.

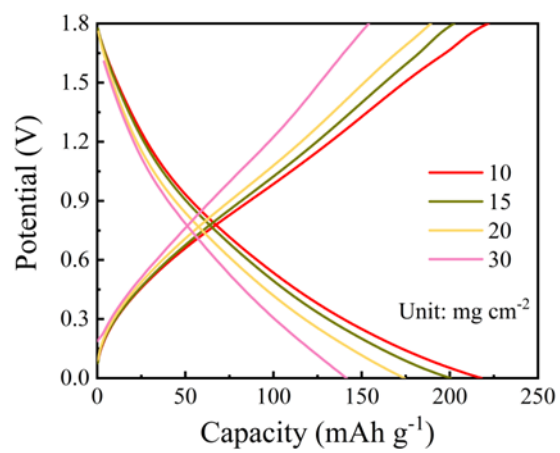


Figure S17. Specific capacities of CS-750 cathode at different mass loadings.

Table S2. Comparison of electrochemical performances of recently reported carbon cathodes for ZHCs.

Carbon electrode	Capacity (mAh g ⁻¹)	Energy density (Wh kg ⁻¹)	Cycling performance	References
Carbon nanosheet	204.7@ 0.1 A g ⁻¹	143	95.5% (200, 000 cycles)	[1]
HPC	206.7@0.2 A g ⁻¹	153.4	100% (50, 000 cycles)	[2]
2D carbon nanosheet	111.0@0.1 A g ⁻¹	109.5	92.7% (50, 000 cycles)	[3]
Carbon Sphere	174.7@0.1 A g ⁻¹	129.3	96% (10, 000 cycles)	[4]
Porous carbon	149@0.2 A g ⁻¹	119	91% (10, 000 cycles)	[5]
HOF derived carbon	132@1 A g ⁻¹	117.5	90% (10, 000 cycles)	[6]
Mesoporous carbon	176@0.5 A g ⁻¹	188	78% (40, 000 cycles)	[7]
3D carbon cathode	133.5@1 A g ⁻¹	119.7	92% (20, 000 cycles)	[8]
OLDC	103@0.5 A g ⁻¹	136.3	91% (20, 000 cycles)	[9]
Spongy HPC	182.6@0.1 A g ⁻¹	292.2	96.2% (10, 000 cycles)	[10]
N-doped HPC	164.2@0.1 A g ⁻¹	128.5	90.3% (30, 000 cycles)	[11]
Co-doped carbon	189.3@0.1 A g ⁻¹	160	92.5% (6, 000 cycles)	[12]
CS-750	262.8@0.2 A g⁻¹	160.8	93.2% (200, 000 cycles)	This work

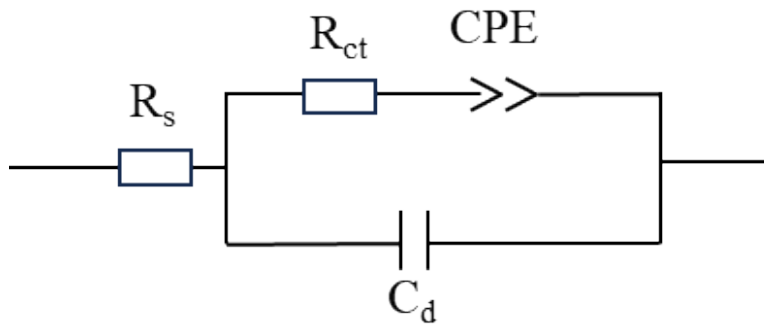


Figure S18. The equivalent resistance of Nyquist plot (R_s : internal resistance of the electrode, R_{ct} : charge transfer resistance, CPE : constant phase angle element, C_d : electrical double layer capacity)

Table S3. Comparison of electrochemical parameters of CS- x electrode in charge/discharge process.

Sample	R_s	R_{ct}	τ_0 (s)	σ ($\Omega \text{ s}^{-0.5}$)	$D_{Zn^{2+}} \times 10^{-21}$ ($\text{cm}^2 \text{ s}^{-1}$)
CS-700	2.8	21.5	41.6	22.4	2.3
CS-750	1.8	9.2	22.7	12.1	8.4
CS-800	2.2	15.3	30.3	18.8	3.5

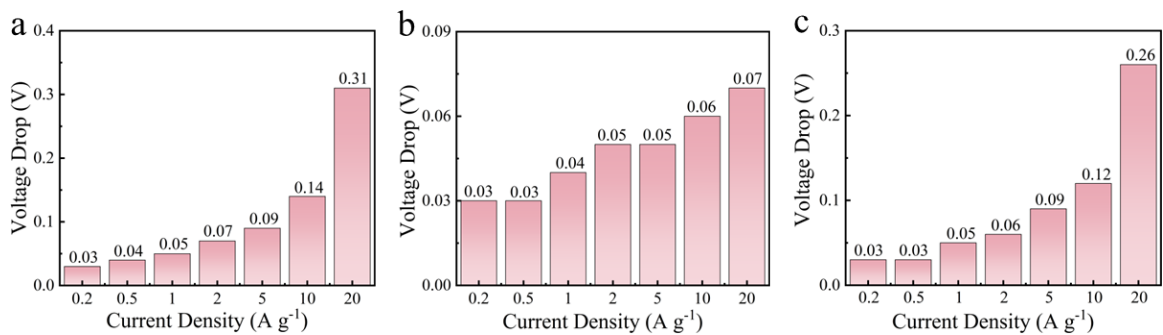


Figure S19. The voltage drop of CS-x electrode: (a) CS-700, (b) CS-750 (b) (c) CS-800.

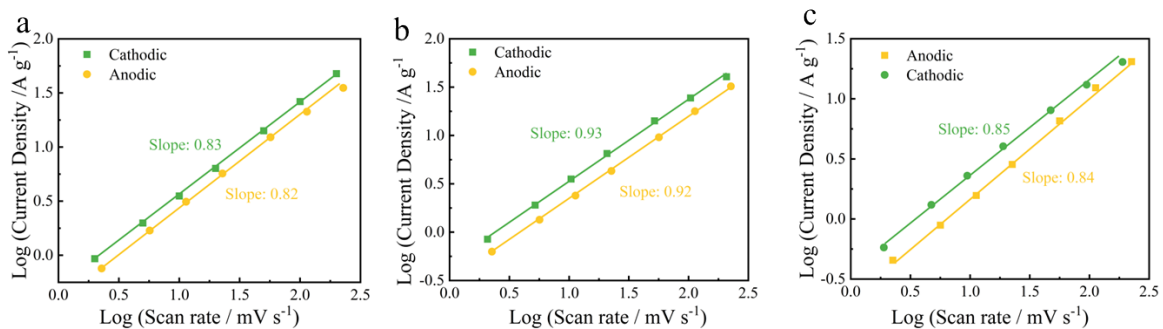


Figure S20. *b* value for CS-x electrode: (a) CS-700 (b) CS-750 (c) CS-800.

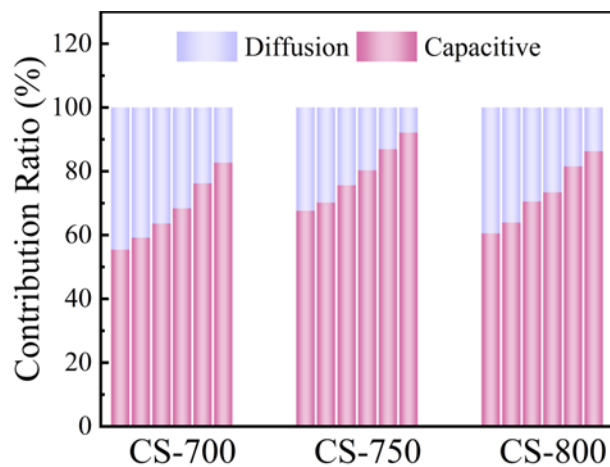


Figure S21. Capacitive and diffusion-controlled contribution ratio of CS-x devices at different scan rate 5, 10, 20, 50, 100, 200 mV s⁻¹.

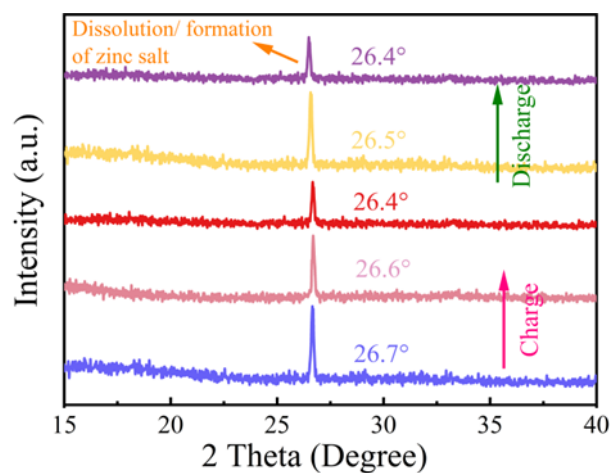


Figure S22. XRD patterns of CS-750 cathode at different charging and discharging points.

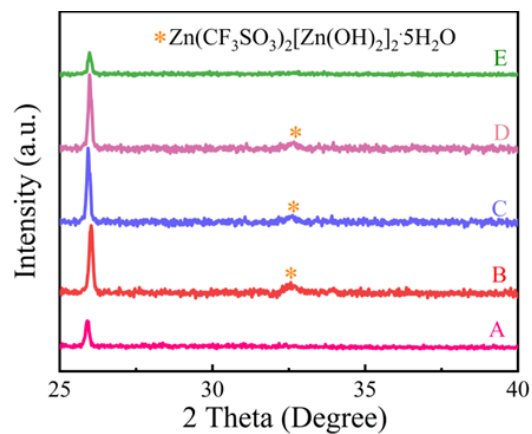


Figure S23. XRD patterns of CS-750 cathode at different discharge point (A, B, C) and charge point (D, E)

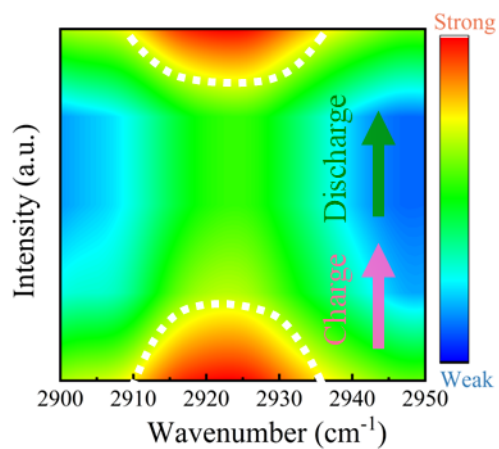


Figure S24. Ex-situ FT-IR spectra of CS-750 cathode at different charge/discharge points.

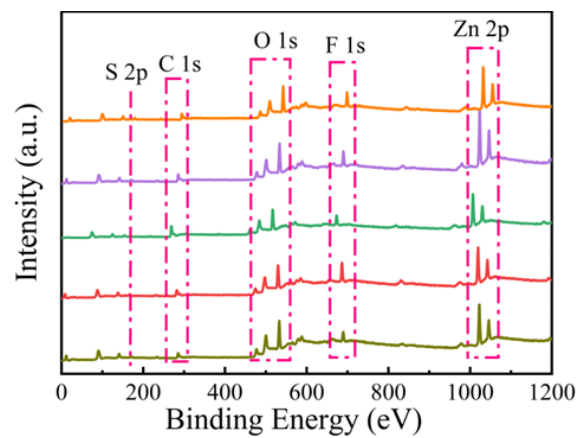


Figure S25. XPS spectra of CS-750 cathode at different charge and discharge points.

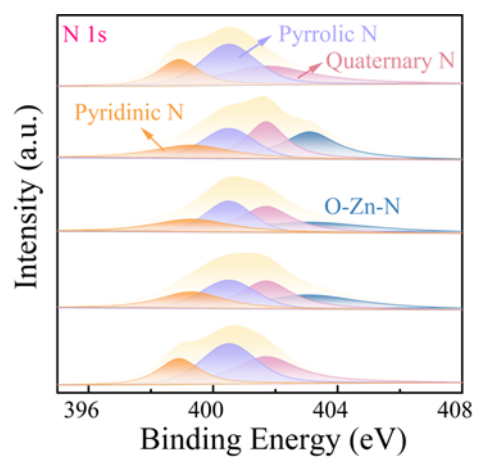


Figure S26. XPS spectra of N 1s at various charging-discharging points of CS-750 cathode.

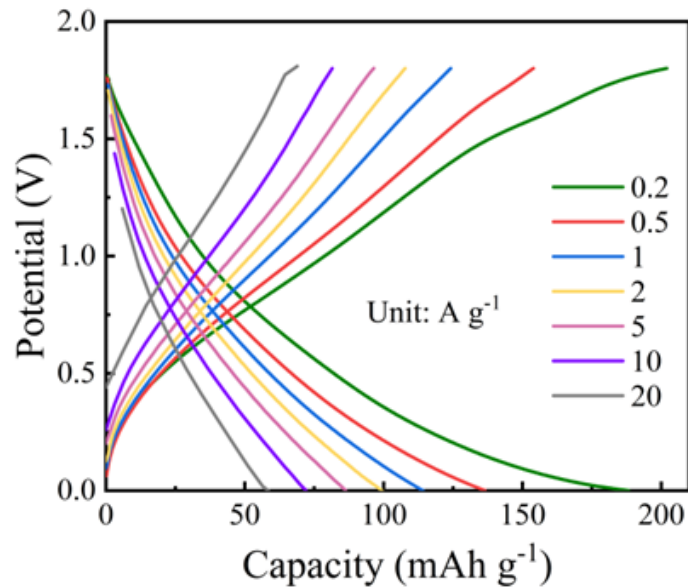


Figure S27. GCD curves of CS-750 cathode using 3M $\text{Zn}(\text{CF}_3\text{SO}_3)_2$ -DMF electrolyte at different current densities from 0.2 A g^{-1} to 20 A g^{-1}

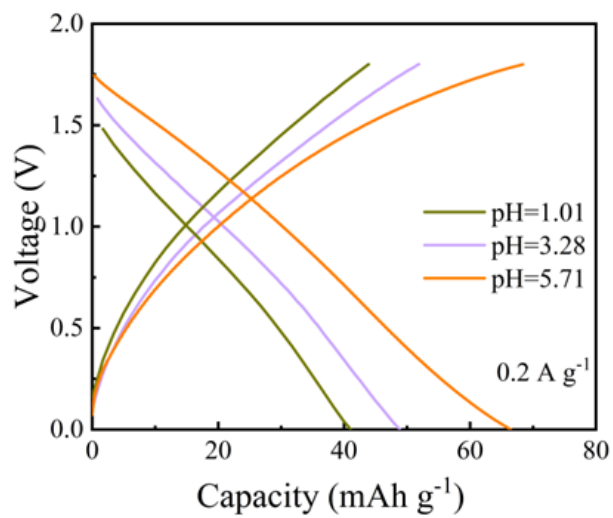


Figure S28. GCD curves of CS-750 cathode with the electrolyte at different pH value.

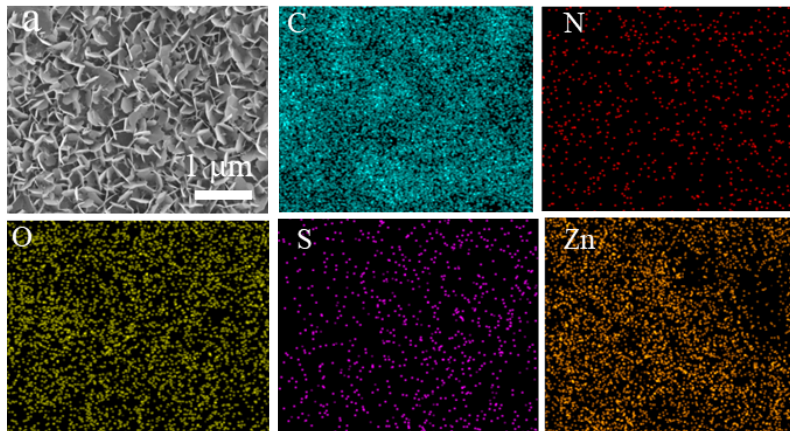


Figure S29. SEM images and EDS mapping of CS-750 cathode at 0 V discharge state.

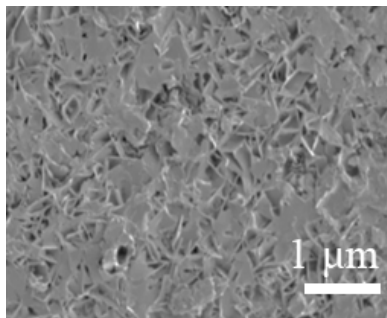


Figure S30. SEM image of CS-750 cathode at 1.8 V charge state.

References

1. F. Wei, H. Zhang, X. Hui, Y. Lv, S. Ran and X. Liu, *J. Power Sources*, 2023, **554**, 232348.
2. Z. Yang, X. Chang, H. Mi, Z. Wang, J. Gao, X. Xiao, F. Guo, C. Ji and J. Qiu, *J. Colloid Interface Sci.*, 2024, **658**, 506-517.
3. G. Lou, G. Pei, Y. Wu, Y. Lu, Y. Wu, X. Zhu, Y. Pang, Z. Shen, Q. Wu, S. Fu and H. Chen, *Chem. Eng. J.*, 2021, **413**, 127502.
4. P. Liu, W. Liu, Y. Huang, P. Li, J. Yan and K. Liu, *Energy Storage Mater.*, 2020, **25**, 858-865.
5. D. Wang, Z. Pan and Z. Lu, *Microporous Mesoporous Mater.*, 2020, **306**, 110445.
6. H. Fan, S. Zhou, Q. Li, G. Gao, Y. Wang, F. He, G. Hu and X. Hu, *J. Colloid Interface Sci.*, 2021, **600**, 681-690.
7. G.-H. An, *Appl. Surf. Sci.*, 2020, **530**, 147220.
8. H. Fan, X. Hu, S. Zhang, Z. Xu, G. Gao, Y. Zheng, G. Hu, Q. Chen, T. S. AlGarni and R. Luque, *Carbon*, 2021, **180**, 254-264.
9. H. Li, P. Su, Q. Liao, Y. Liu, Y. Li, X. Niu, X. Liu and K. Wang, *Small*, 2023, **19**, 2304172.
10. X. Zhang, Y. Zhang, J. Qian, Y. Zhang, L. Sun and Q. Wang, *Nanoscale*, 2022, **14**, 2004-2012.
11. D. Jia, Z. Shen, W. Zhou, Y. Li, J. He, L. Jiang, Y. Wei and X. He, *Chem. Eng. J.*, 2024, **485**, 149820.
12. Y. Zhang, X. Li, Y. Li, X. Zhang, D. Yu, C. Chen and G. Zhao, *Electrochim. Acta*, 2023, **447**, 142114.